ACS APPLIED MATERIALS & INTERFACES

Subscriber access provided by Imperial College London | Library

Surfaces, Interfaces, and Applications

3D-Printed Surfaces Inspired by Bi-Gaussian Stratified Plateaus

Songtao Hu, Xiaobao Cao, Tom Reddyhoff, Debashis Puhan, Weifeng Huang, Xi Shi, Zhike Peng, and Daniele Dini

ACS Appl. Mater. Interfaces, **Just Accepted Manuscript** • DOI: 10.1021/acsami.9b04020 • Publication Date (Web): 15 May 2019

Downloaded from http://pubs.acs.org on May 23, 2019

Just Accepted

"Just Accepted" manuscripts have been peer-reviewed and accepted for publication. They are posted online prior to technical editing, formatting for publication and author proofing. The American Chemical Society provides "Just Accepted" as a service to the research community to expedite the dissemination of scientific material as soon as possible after acceptance. "Just Accepted" manuscripts appear in full in PDF format accompanied by an HTML abstract. "Just Accepted" manuscripts have been fully peer reviewed, but should not be considered the official version of record. They are citable by the Digital Object Identifier (DOI®). "Just Accepted" is an optional service offered to authors. Therefore, the "Just Accepted" Web site may not include all articles that will be published in the journal. After a manuscript is technically edited and formatted, it will be removed from the "Just Accepted" Web site and published as an ASAP article. Note that technical editing may introduce minor changes to the manuscript text and/or graphics which could affect content, and all legal disclaimers and ethical guidelines that apply to the journal pertain. ACS cannot be held responsible for errors or consequences arising from the use of information contained in these "Just Accepted" manuscripts.

is published by the American Chemical Society. 1155 Sixteenth Street N.W., Washington, DC 20036

Published by American Chemical Society. Copyright © American Chemical Society. However, no copyright claim is made to original U.S. Government works, or works produced by employees of any Commonwealth realm Crown government in the course of their duties.

3D-Printed Surfaces Inspired by Bi-Gaussian Stratified Plateaus

Songtao Hu,[†] Xiaobao Cao,[‡] Tom Reddyhoff,[§] Debashis Puhan,[§] Weifeng Huang,[⁄⁄] Xi Shi,[*,†] Zhike Peng,[*,†] and Daniele Dini[§]

[†] State Key Laboratory of Mechanical System and Vibration, Shanghai Jiao Tong University, Shanghai 200240, China
[‡]Department of Chemistry and Applied Biosciences, ETH Zurich, Zurich 8093, Switzerland
[§]Department of Mechanical Engineering, Imperial College London, London SW7 2AZ, UK
[⁄⁄] State Key Laboratory of Tribology, Tsinghua University, Beijing 100084, China

ABSTRACT: Wettability of artificial surfaces is attracting increasing attention for its relevant technological applications. Functional performance is often achieved by mimicking topographical structures found in natural flora and fauna, however, surface attributes inspired by geological landscapes have so far escaped attention. We reproduced a stratified morphology of plateaus with a bi-Gaussian height distribution using a 3D direct laser lithography. The plateau-inspired artificial surface exhibits a hydrophobic behavior even if fabricated from a hydrophilic material, giving rise to new wetting mechanism that divides the well-known macroscopic Wenzel and Cassie states into four sub-states. We have also successfully applied the plateau-inspired structure to droplet manipulation.

KEYWORDS: artificial surface, stratified morphology, 3D laser lithography, wettability, droplet manipulation

■ INTRODUCTION

Wettability has been a research hotspot in surface engineering in recent years, offering exciting opportunities for numerous emerging applications such as self-cleaning, transportation, antifogging, anti-icing, antireflection, drag reduction, energy harvest, biosensor, etc.[1−8] To achieve such fascinating capabilities, the combination of micro-/nanotopographical structures and chemical modification on solid surfaces has been demonstrated as an optional strategy to markedly alter surfaces' wetting behavior. More precisely, the wettability is not merely dependent on the chemical interaction of a solid-liquid interface but mostly on the superficial morphology of micro-/nanostructures.[9] Considerable inspiration in this area has been gained from natural surfaces including those found on flora[10] and fauna[11], with the intent to mimic salient micro/nanostructures to achieve similar physical traits and functional performances. These artificial biomimetic structures were usually encouraged to exhibit a multiscale (fractal or hierarchical) feature with the scenario of either a random distribution[12] or an extraordinarily ordered pattern[13], in which distinctive (e.g., crown-like[14,15] and mushroom-like[16,17]) submicro-/nanostructures were fabricated

atop the underlying microstructures like pillars and cones.

In the present work, we report a new two-layer artificial structure inspired by the bi-Gaussian stratified morphology of geological landscapes, thereby extending the scope of natural inspiration to non-biological examples. Similar to the fractal notion inspired by geological landscapes like coastlines,[18] Figure 1a. i shows a typical bi-Gaussian stratified morphology of plateaus in the Grand Canyon National Park taken by Google Earth Pro (Google LLC). This series of mountains was generated during a past diastrophism, yielding deep valleys heavily interpenetrated by high peaks, which were subsequently truncated by environmental actions of wind and rain so as to form flat plateaus. This inspires a peculiar topography (see Figure 1a. ii) in which a large roughness-scale surface (lower component) is intersected by another surface with a small roughness scale (upper component). Each component independently follows a Gaussian distribution in terms of surface heights to satisfy a randomness requirement so as to insure widespread applicability. In contrast with the common multiscale (fractal or hierarchical) feature exhibiting self-similarity at different scales, the plateau-inspired one emphasizes the stratified property (i.e., selectively retaining the lower height on any node in the combination of the upper and lower components) at a single scale.

This bi-Gaussian stratified morphology widely exists on engineering surfaces (see Figure 1b) as a result of a multi-stage abrasive manufacturing process[19], particularly on surfaces those have undergone a material wear in service[20]. However, most researchers have been puzzled by the apparently non-Gaussian distribution, overlooking the real-life scenario of a bi-Gaussian stratified property. Recently, the bi-Gaussian stratified feature has been differentiated from the non-Gaussian feature, and has begun to be investigated from morphological and functional points of view. Interestingly, functional performances of the two components are clearly defined in comparison to the conventional perspective of a single stratum. Taking the tribological field as an example, the upper component plays roles in load bearing and wear resistance while the lower component serves as lubricant reservoirs and debris traps.[20] So far, the bi-Gaussian stratified idea is starting to render its excellent capability in revealing and optimizing interfacial lubrication, wear, wettability and manufacturing.[19–21]

In this work, we focused on proposing a two-layer artificial surface (see Figures 1c, 1d and 1e) consisting of micro-fabricated pillars inspired by a bi-Gaussian stratified morphology discovered in landscapes and industry, starting from a hydrophilic material while finally exhibiting a macroscopical hydrophobicity. In particular, we investigated how the two-layer artificial structure, respecting a bi-Gaussian stratified distribution in terms of pillar heights, can impact the wetting behavior by establishing a theoretical static contact angle model based on the well-known Wenzel and Cassie theories. The implementation of such artificial surfaces could be of significant technological interest because it could provide a feasible approach to control wettability by optimizing the arrangement of pillar heights instead of decorating the shape of pillars appreciated in precious studies[14–17]. Notably, this study is a preliminary attempt to utilize the inspiration from bi-Gaussian stratified morphology in the realm of wettability. As a further outlook, our particular two-layer arrangement can offer a flexible choice to tailor omniphobicity[17] if the two layers are designed with different textures or made of different materials. This study, in addition, provides

valuable insights on the design and manufacturing of conventional engineering components because of the widespread presence of a bi-Gaussian stratified morphology in industry.

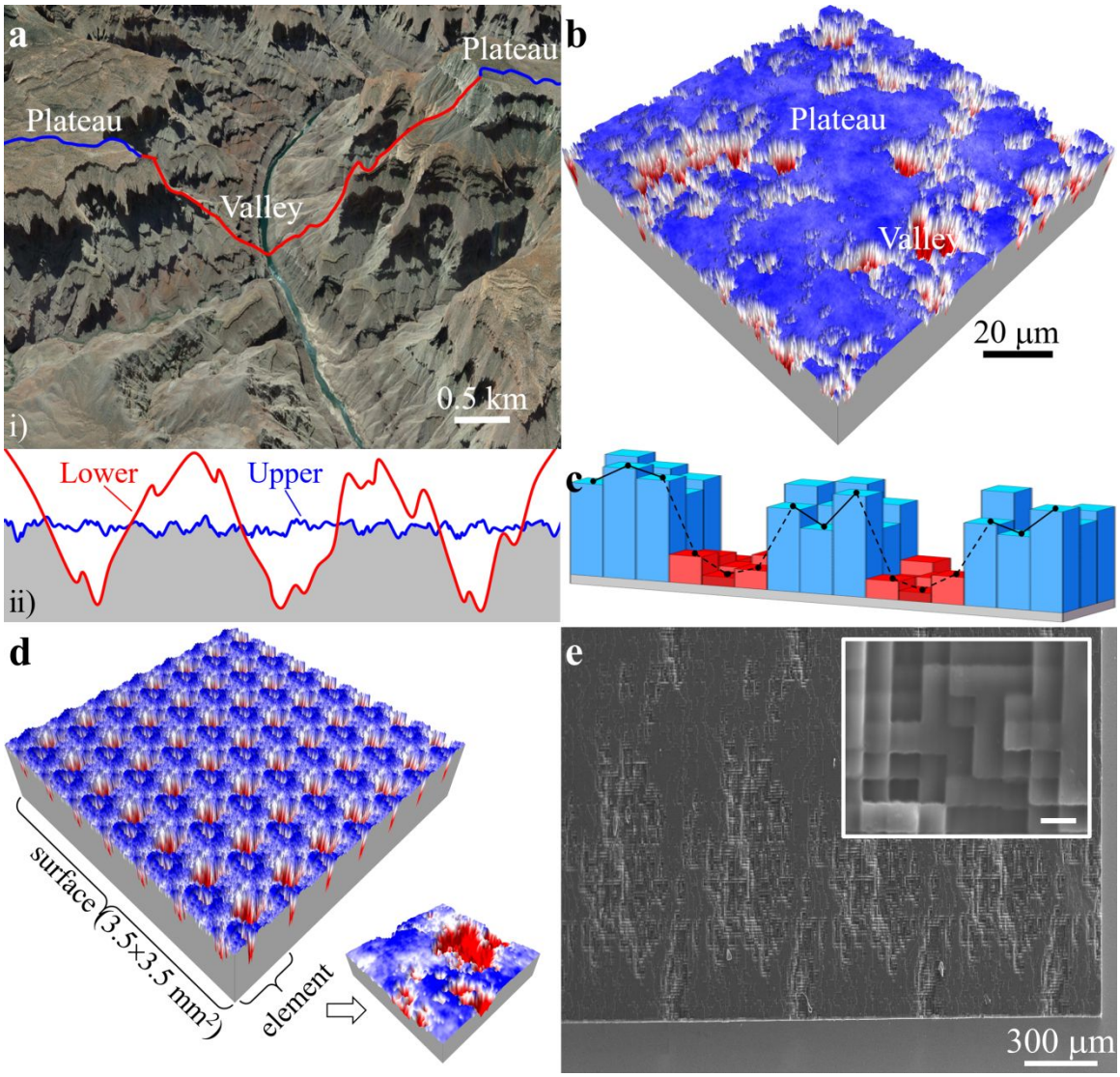


Figure 1. (a) Bi-Gaussian stratified morphology of plateaus observed in the Grand Canyon National Park (i) and its 2D schematic (ii). (b) Bi-Gaussian stratified morphology observed on engineering surfaces. (c) Two-layer artificial structure composed of pillars following two height distributions inspired by a bi-Gaussian stratified morphology. (d) Design of a plateau-inspired artificial surface as a matrix of 7×7 bi-Gaussian stratified elements. (e) Plateau-inspired artificial surface made of IP-S photoresist on a glass substrate by means of 3D direct laser lithography using NanoScribe Photonic Professional System (inset: pillars with scale bar 10 μm).

■ EXPERIMENTAL SECTION

A plateau-inspired artificial surface with a size of 3500×3500 μm^2 was purposely designed as a 7×7 matrix consisting of prescribed bi-Gaussian stratified elements (see Figures 1d and S2), each

element being composed of 64×64 pillars. Such a matrix design was employed to eliminate the repetitive error when we measured the static contact angles of water droplets at different contact positions on each pure plateau-inspired artificial surface (see Figure S2). Moreover, with this matrix design it was possible to create a gradient plateau-inspired artificial structure via a proper combination of different types of bi-Gaussian stratified elements (see Figure S2) in section APPLICATION. In each bi-Gaussian stratified element, the pillar height was designed to follow a bi-Gaussian stratified distribution, thus yielding a two-layer arrangement. The pillar heights were controlled by setting prescribed bi-Gaussian stratified indexes including the autocorrelation function (ACF) length, the root-mean-square height of pillars on the upper layer *Spq*, the root-mean-square height of pillars on the lower layer *Svq*, and the proportion of pillars on the upper layer *Smq* (clearly defined in "Characterization and Simulation of Bi-Gaussian Stratified Morphology" in Supporting Information).

Samples were designed so that each pure plateau-inspired artificial surface (see P1−P6 in Figures S2 and 2a) exhibited a single bi-Gaussian stratified element. P1 was regarded as the fundamental case where ACF lengths in the *x* and *y* directions, *Spq*, *Svq* and *Smq* were set to 7.9 μm, 1 μm, 10 μm and 50 %; P2 (ACF lengths in the *x*- and *y*- directions: 250 μm), P3 (*Spq*: 5 μm), P4 (*Svq*: 2 μm) and P5 (*Smq*: 80 %) were added to explore the distinguished wettability induced by different bi-Gaussian stratified indexes, revealing the inherent wetting mechanism of a bi-Gaussian stratified morphology. A deviation of ACF lengths was also set between the *x* and *y* directions in P6 (ACF lengths were set to 250 μm and 7.9 μm in the *x* and *y* directions, respectively) to induce a directional wettability, which has been a fascinating topic on anisotropic surfaces.[13] In addition, a flat reference was preset as the ideal smooth surface to obtain the intrinsic contact angle in Young's equation.

These designed pure plateau-inspired artificial surfaces were numerically generated by the simulation method of bi-Gaussian stratified morphologies (see Figure S1b) programmed in Matlab (Mathworks Inc.), and were then fabricated by a 3D direct laser lithography attaching IP-S photoresist (NanoScribe GmbH) to an ITO coated fused silica by means of a two-photon polymerization on Photonic Professional System (NanoScribe GmbH). In comparison to other strategies of tailoring topographical structures such as physical/chemical vapor deposition,[22] sol-gel,[23] self-assembled monolayer[24] and femtosecond laser,[2] the NanoScribe system can be regarded as the most precise rapid prototyping technology to realize 3D structures at a micrometric level even at a nanoscale in the up-to-date applications of mechanical metamaterials,[25] optics,[26] photonics,[27] etc. To our knowledge, this technology, recently, started to be employed as a powerful tool in wettability investigation.[14,17,28−30]

Conventionally, a program is required to convert the matrix format generated by Matlab into the recognizable stereolithography format (.stl).[29] However, in a case with the size of mm^3, this "mesh to solid" converter will lead to a file size of hundreds of MB or even several GB, exhausting the computer resource.[28] In this study, as the bi-Gaussian stratified notion was only adopted to optimize the arrangement of pillar heights rather than the shape of pillars, the matrix format has been converted into a grayscale format, serving as the input of the NanoScribe system. During the fabrication, IP-S photoresist was exposed to a 780-nm femtosecond laser through an oil-immersion

objective (numerical aperture = 0.8). The interface between the photoresist and the substrate was searched and the laser was then commanded to write 0.5 μm beneath the interface, ensuring a good adhesion of the printed structures on the glass substrate. The laser writing was conducted at a speed of 100 mm·s^{-1} with a power of 110 mW. The fabrication was then developed for 20 min in a SU-8 Developer (MicroChem Corp) and rinsed in isopropyl alcohol and deionized water. Thanks to the laser writing process, two-layer artificial structures made of IP-S photoresist were well attached on glass substrates (see Figure 2b) in good agreement with the initial design.

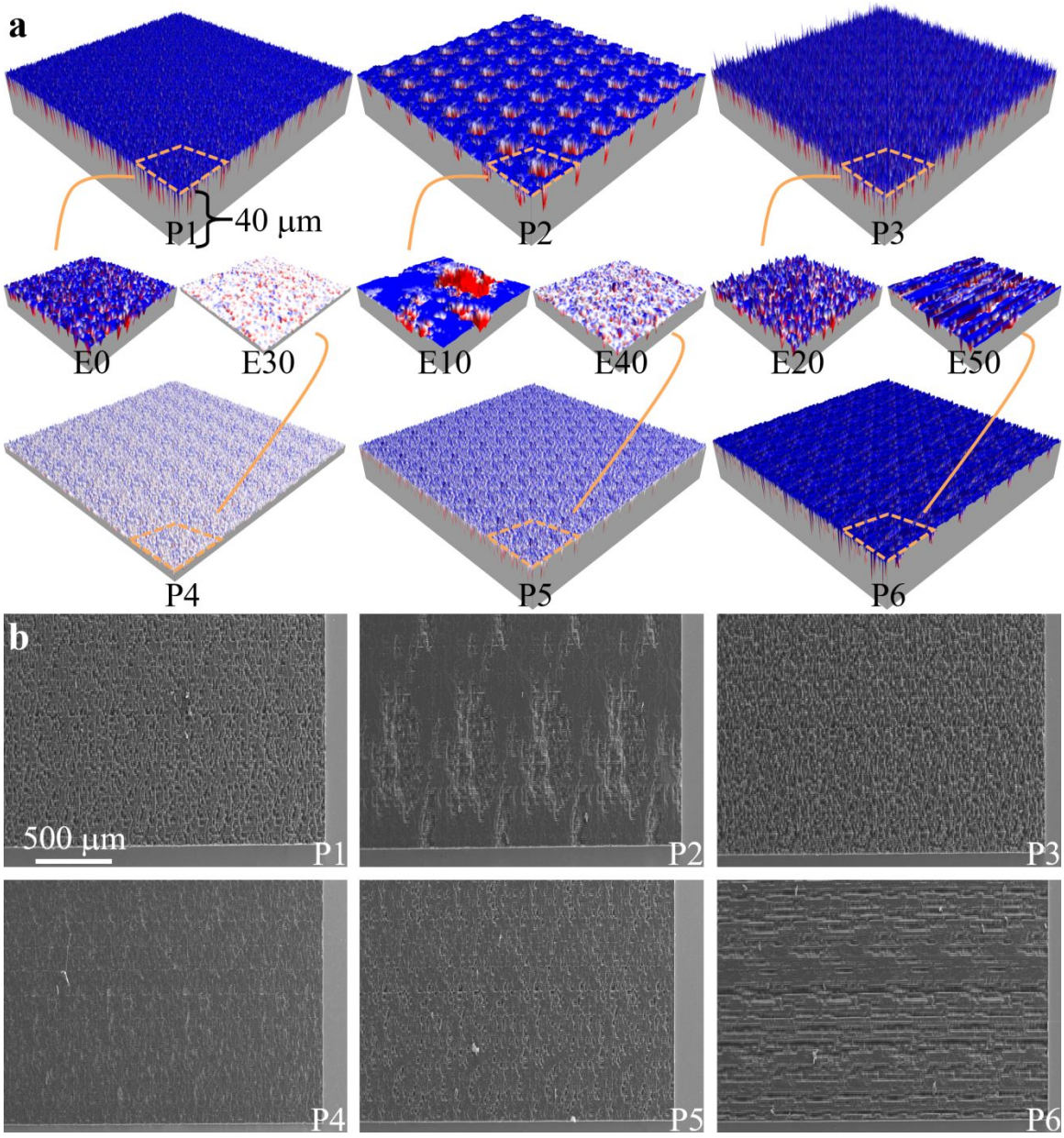


Figure 2. (a) Visualization of the designed pure plateau-inspired artificial surfaces: P1 vs. P2 to show the effect of ACF length; P1 vs. P3 to show the effect of *Spq*; P1 vs. P4 to show the effect of *Svq*; P1 vs. P5 to show the effect of *Smq*; P1 vs. P6 to show the effect of a directional difference in

ACF lengths; elements E0, E10, E20, E30, E40 and E50 illustrated in Table S1. (b) Scanning electron microscope images of the fabricated pure plateau-inspired artificial surfaces.

To characterize the wettability of plateau-inspired artificial surfaces, the static contact angle, serving as a key evaluation index, for a 4-μL droplet of deionized water was measured by Rame-Hart Contact Angle Goniometer (Rame-Hart Instrument Co.) via a sessile drop method under controlled temperature (20 °C) and relative humidity (45 %). Each contact angle was captured 30 sec after the droplet contacted the target artificial surface in order to insure equilibrium. The measurement was conducted five times on the same plateau-inspired artificial surface to confirm excellent repeatability.

RESULTS AND DISCUSSION

Gratifyingly, the static contact angles (see Figure 3a) on plateau-inspired artificial surfaces were greater than that on the flat reference (67.2 °), even reaching a hydrophobic level. This is a remarkable result that verifies the function of a two-layer arrangement to convert the initial hydrophilicity into a macroscopic hydrophobicity. Referring to the Wenzel model, a roughness will intensify the inherently hydrophilic characteristic. The converse effect in this study is attributed to the Fakir effect of pillars.[31] Combined with peculiar topological (mushroom-like or crown-like) structures fabricated atop the pillars, this Fakir effect can even convert hydrophilicity into superhydrophobicity.[14–17] In comparison to a single Gaussian arrangement (see Figure S5), a bi-Gaussian stratified one exhibited an enhanced water repellency due to the suspending effect of the plateaus (i.e., upper component) and the air reservoirs formed by the valleys (i.e., lower component). It is important to highlight that the prescribed bi-Gaussian stratified indexes, in terms of ACF lengths, *Spq*, *Svq* and *Smq*, are crucial factors in determining the fraction of solid-liquid and gas-liquid interfaces. More precisely, a greater ACF length (see P2 vs. P1) differentiates the interpenetrated pillars,[21] thus forming wide valleys to trap the droplet to render a smaller contact angle. A greater *Spq* (see P3 vs. P1) indicates a rougher upper layer, enabling more of that layer to become gas traps to decrease the fraction of the solid-liquid interface so as to present a greater contact angle. A smaller *Svq* (see P4 vs. P1) decreases the volume of trapped gas, resulting in a smaller contact angle. A greater *Smq* (see P5 vs. P1) decreases the proportion of the lower layer, thereby diminishing the volume of gas traps to yield a smaller contact angle. However, the difference in contact angle here is smaller than the circumstance of P4 vs. P1 because an increased proportion of the upper layer leads to an increased fraction of the gas-liquid interface, thus providing an opposite augmentation to the contact angle. A directional deviation of contact angle is acquired (see P6) by setting different ACF lengths between the *x* and *y* directions.

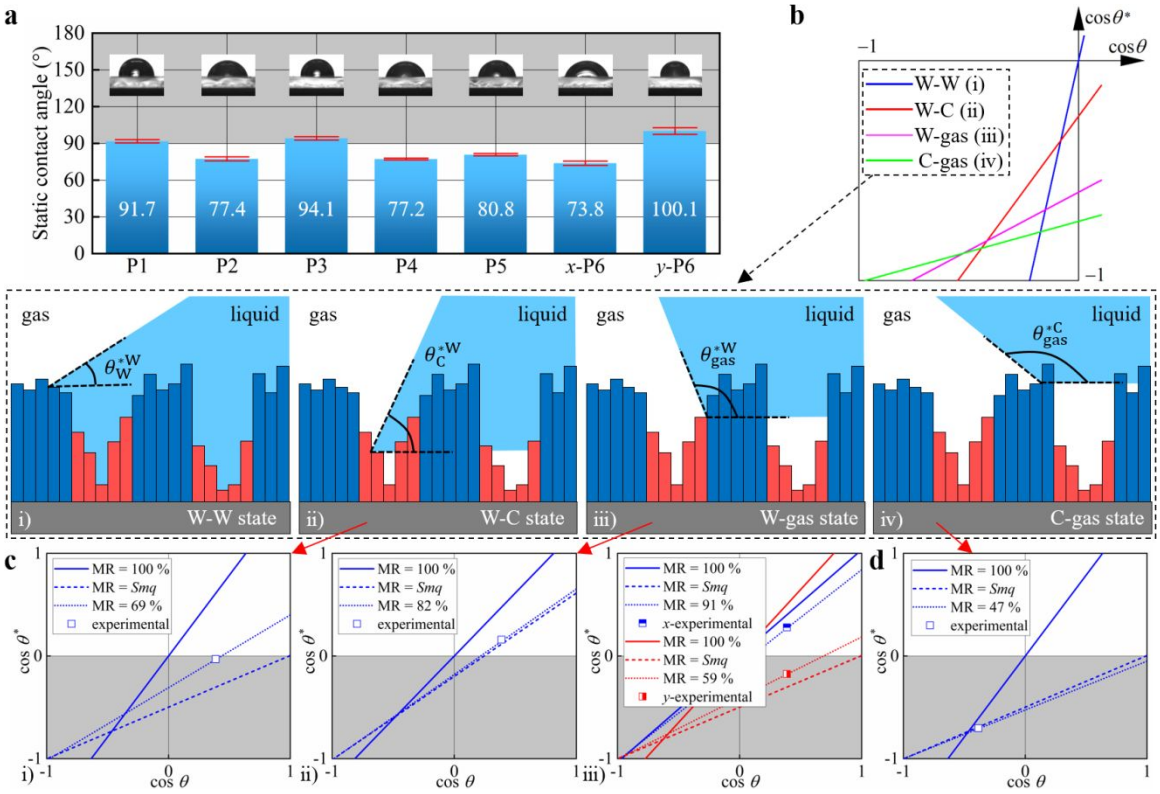


Figure 3. (a) Static contact angles on the pure plateau-inspired artificial surfaces with different bi-Gaussian stratified indexes. (b) Theoretical static contact angle model for a bi-Gaussian stratified morphology, introducing four different wetting states, (ⅰ) W-W, (ⅱ) W-C, (ⅲ) W-gas, and (ⅳ) C-gas states, eqs 1−4. (c) Theoretical and experimental relationships between apparent contact angles and intrinsic contact angles on the pure plateau-inspired artificial surfaces, (ⅰ) P1, (ⅱ) P5, and (ⅲ) P6, where an ideal smooth surface was employed to obtain the intrinsic contact angle. (d) Theoretical and experimental relationship between apparent contact angle and intrinsic contact angle on a pure plateau-inspired artificial surface made of hydrophobic polydimethylsiloxane, having the same bi-Gaussian stratified indexes with P1.

To further explain how a plateau-inspired artificial surface can affect the wettability from a theoretical point of view, we established a static contact angle model based on the well-known Wenzel and Cassie theories (see "Bi-Gaussian Stratified Wetting Model" in Supporting Information) rendered as

$$\cos\theta_{\mathrm{W}}^{*\mathrm{W}} = (1+Sdr)\times\cos\theta, \qquad \text{when MR} = 100\,\%; \tag{1}$$

$$\cos\theta_{\mathrm{C}}^{*\mathrm{W}} = (1+Sdr_{\mathrm{MR}})\times\mathrm{MR}\times\cos\theta+\mathrm{MR}-1, \qquad \text{when MR} \in (Smq, 100\,\%); \tag{2}$$

$$\cos\theta_{\mathrm{gas}}^{*\mathrm{W}} = (1+Sdr_{Smq})\times Smq\times\cos\theta+Smq-1, \qquad \text{when MR} = Smq; \tag{3}$$

$$\cos\theta_{\text{gas}}^{*\text{C}} = (1 + Sdr_{\text{MR}}) \times \text{MR} \times \cos\theta + \text{MR} - 1, \qquad \text{when MR} \in (0, Smq)\,. \tag{4}$$

Herein θ is the intrinsic contact angle on an ideal smooth surface, which is associated with the solid surface free energy, liquid surface tension and solid-liquid interfacial energy in Young's equation. And θ^* is the apparent contact angle on a rough surface affected by the roughness factor r (see eq S5, the ratio of the real area to the projected one to indicate an area extension) and the fraction of the solid-liquid interface f (see eq S6). Material ratio (MR), indicating the probability to find a pillar above a certain height (see eq S2), was employed to define the boundary between the wetted and unwetted regions. The roughness factor r was evaluated by the developed interfacial area ratio Sdr (see eq S7), whose subscript means that the value of Sdr should be calculated within the pillars above an intersecting plane defined by the employed MR (instead of being calculated over all nodes required in ISO 25178). Consequently, eqs 1−4 divide the macroscopic Wenzel and Cassie states into four different sub-states on a plateau-inspired artificial surface (see Figures 3b and S6). In the first state, the MR is equal to 100 % (see Figure S6a) with the lower and upper layers in the Wenzel state (see Figures 3b. i and S6b. i). In the second state, the MR decreases from 100 % and stops at a value within the interval of (Smq, 100 %) (see Figure S6a), leading to the upper layer in the Wenzel state while the lower component in the Cassie state (see Figures 3b. ii and S6b. ii). In the third state, the MR is exactly equal to Smq (see Figure S6a), indicating that the upper layer is in the Wenzel state while the lower layer is in a completely gaseous environment (see Figures 3b. iii and S6b. iii). In the fourth state, the MR reaches a tiny value within the interval of (0, Smq) (see Figure S6a) where the lower layer is in the gas environment while the upper layer has entered into the Cassie state (see Figures 3b. iv and S6b. iv). Hence, the superscript and subscript of θ^* in eqs 1−4, respectively, represent the wetting states of the upper and lower layers with "W", "C" and "gas" relating to Wenzel state, Cassie state and gas environment. This bi-Gaussian stratified wetting model is suitable not only for the two-layer artificial surface in this work but also conventional engineering surfaces with a bi-Gaussian stratified morphology in industry, such as automotive cylinder liners. It is important to underline that the value of MR is, of course, dependent on the physicochemical attributes of solid and liquid as well as environmental factors, making it a challenge to be theoretically calculated. Nevertheless, our model, unlike the Wenzel and Cassie models, can be used as a probe to estimate the wetting statuses of the two component layers. The C-gas state should be the highest energy state in comparison to the other three from a thermodynamic point of view. It therefore would transfer into the W-gas, W-C, or W-W state after a sufficient duration of time,[32] or if disturbed by ambient factors such as mechanical process, evaporation, and condensation.[33]

By applying the bi-Gaussian stratified wetting model to the previously measured static contact angles, the theoretical and experimental relations between apparent contact angles and intrinsic contact angles were depicted in Figures 3c and S7. In P1−P4, the dotted line across the experimental data is surrounded by the solid (MR = 100 %) and the dashed (MR = Smq) lines, indicating a W-C wetting state (see Figure 3c. i). In P5, the dotted line is very close to the dashed line, thus approaching a W-gas wetting state (see Figure 3c. ii). When the dotted line is below the dashed

line, the wetting state has entered into a C-gas state, which can be observed in another P1 case made of hydrophobic polydimethylsiloxane (see Figure 3d). In such case, a mold was first fabricated on a glass substrate by the NanoScribe system with the hydrophilic IP-S photoresist; then, the polydimethylsiloxane was used to copy the morphology from the resulting mold, thereby generating the other P1 case, however now, composed by a hydrophobic material. The intrinsic contact angle on a smooth polydimethylsiloxane surface is 112.6 °, and the apparent contact angle on P1 made of polydimethylsiloxane is 134.6 °, as displayed in Figure S12. In P6 (see Figure 3c. iii), the bi-Gaussian stratified wetting model has been improved to a 2D formation to capture the directional deviation caused by an ACF-length difference between the *x* and *y* directions.

APPLICATION

In this section, the inspiration of a bi-Gaussian stratified morphology to mimic two-layer artificial structures was employed in the application of droplet manipulation, which has been widely investigated in areas such as adhesion control from lotus leaf to rose petal,[2] and microfluidics based on hydrophobic-hydrophilic transitions.[34] To realize the droplet transportation based on a hydrophobic-hydrophilic transition, a gradient plateau-inspired artificial surface was designed (see Figure 4a) by a proper combination of different types of bi-Gaussian stratified elements, and was then realized using the NanoScribe system (see Figure 4b). Herein, bi-Gaussian stratified gradients were created (see Figures S2 and S3) in terms of ACF length (G1, ACF lengths in the *x* and *y* directions ranging from 7.9 μm to 250 μm), *Spq* (G2, *Spq* ranging from 1 μm to 5 μm), *Svq* (G3, *Svq* ranging from 10 μm to 2 μm), *Smq* (G4, *Smq* ranging from 5 % to 95 %) and directional difference (G5, ACF length in the *x* direction ranging from 7.9 μm to 250 μm in comparison to the constant ACF length in the *y* direction of 7.9 μm). These designed gradient plateau-inspired artificial structures were then made of IP-S photoresist and fabricated on glass substrates (see Figure S4), in good agreement with the initial design.

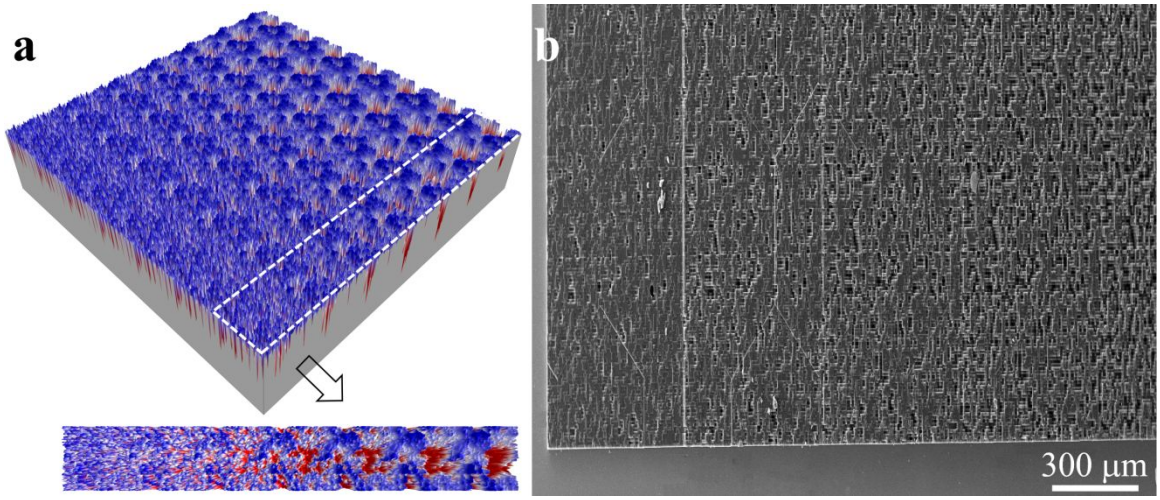


Figure 4. (a) Design of a plateau-inspired artificial surface G1 with an ACF-length gradient (ACF lengths in the *x* and *y* directions ranging from 7.9 μm to 250 μm). (b) Scanning electron microscope images of the fabricated gradient plateau-inspired artificial surface G1.

On a horizontal platform (see Figure 5a), a water droplet instantaneously became asymmetric when it contacted the plateau-inspired artificial surface G1 with an ACF-length gradient (capitals "A" and "B" relating to the surface edges with 7.9-μm and 250-μm ACF lengths), and finally stopped at the position that was away from the central line of the syringe and simultaneously formed a distinguished deviation between the left (83.8 °) and right (78.3 °) contact angles, thus indicating a driving force induced by the preset bi-Gaussian stratified gradient. To better gauge the power of a bi-Gaussian stratified gradient, we continued to pressurize the droplet by reducing the vertical height of the syringe (see Figure 5b). Under an extrusion force, the droplet deformed directionally along the bi-Gaussian stratified gradient (from edge B to edge A) and remained unchanged relative to the edge B, and even broke the inherently spherical shape when it touched the edge A, showing the greater power of the bi-Gaussian stratified gradient in comparison to the extrusion force. We repeated the above squeezing action on a platform tilted by 10 ° (see Figure 5c). The droplet still deformed directionally along the bi-Gaussian stratified gradient, validating that the bi-Gaussian stratified gradient was sufficiently high to resist both the extrusion force and gravity. Similar droplet manipulation can be achieved on plateau-inspired artificial surfaces with a designed gradient in terms of *Spq*, *Svq*, *Smq*, and directional ACF-length difference, as depicted in Figures S8, S9, S10 and S11.

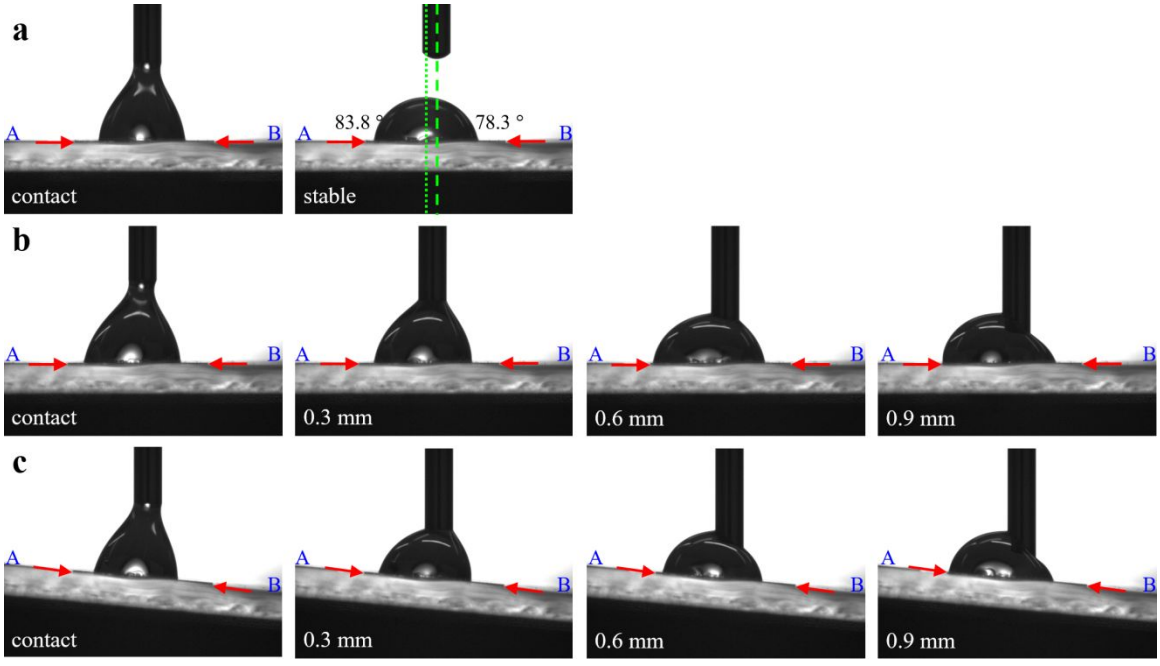


Figure 5. Droplet manipulation by an ACF-length gradient (ACF lengths in the *x* and *y* directions ranging from 7.9 μm to 250 μm) on a plateau-inspired artificial surface G1. (a) Horizontal motion of a water droplet induced by the gradient. (b) Horizontal motion of a water droplet induced by the gradient and an extrusion force arising from the vertical reduction of the syringe: droplet contacted surface, syringe declined 0.3 mm, syringe declined 0.6 mm, and syringe declined 0.9 mm. (c) Motion of a water droplet on a tilted platform with 10 ° induced by the gradient to resist the

extrusion force and the droplet gravity. Arrows indicating the surface edges. Capitals "A" and "B" relating to the surface edges with 7.9-μm and 250-μm ACF lengths. Dashed and dotted lines indicating the centers of the syringe and the droplet.

CONCLUSIONS

In this work, we extended the scope of naturally inspired interface beyond previous studies limited to mimicking flora and fauna. Similar to the famous fractal concept inspired by landscapes such as coastlines, we reported a two-layer artificial surface motivated by plateaus with a bi-Gaussian stratified morphology. 3D direct laser lithography was employed in the fabrication of two-layer artificial surfaces to precisely replicate the interesting plateau morphology, paving a way to explore the wettability on a bi-Gaussian stratified topography. A static contact angle model was developed for a bi-Gaussian stratified morphology in revealing new wetting mechanisms, dividing the well-known macroscopic Wenzel and Cassie states into four sub-states depending on the wetting states of the two component layers. This understanding was employed to produce hydrophobic surfaces out of hydrophilic materials, and was successfully applied to the droplet manipulation for gravity resistance. In the field of interface assembly, the present work can be regarded as a guide to optimize the arrangement of pillar heights instead of solely decorating the shape of pillars appreciated in precious studies. This work also provides valuable insights on the design and manufacturing due to the widespread presence of a bi-Gaussian stratified morphology on conventional engineering components used in industry. As a further outlook, the particular two-layer arrangement can offer a flexible choice to reach omniphobicity when two layers are fabricated from different materials or are decorated with peculiar topological structures.

ASSOCIATED CONTENT

The Supporting Information is available free of charge on the ACS Publications website at DOI: xxxxxxxxxx.

Some more details about surface theories, design of artificial surfaces, fabrication of artificial surfaces, wetting theories, and related figures (PDF)

AUTHOR INFORMATION

Corresponding Authors

*E-mail: xishi@sjtu.edu.cn (X.S.).

*E-mail: z.peng@sjtu.edu.cn (Z.P.).

Notes

The authors declare no competing financial interest.

ACKNOWLEDGEMENTS

This work was supported by China Postdoctoral Science Foundation (2017M621458), and National

Natural Science Foundation of China (11572192, 11632011).

REFERENCES

(1) Furstner, R.; Barthlott, W.; Neinhuis, C.; Walzel, P. Wetting and Self-Cleaning Properties of Artificial Superhydrophobic Surfaces. *Langmuir* **2005**, 21, 956−961.
(2) Long, J.; Fan, P.; Gong, D.; Jiang, D.; Zhang, H.; Li, L.; Zhong, M. Superhydrophobic Surfaces Fabricated by Femtosecond Laser with Tunable Water Adhesion: from Lotus Leaf to Rose Petal. *ACS Appl. Mater. Inter.* **2015**, 7, 9858−9865.
(3) Han, Z.; Feng, X.; Guo, Z.; Niu, S.; Ren, L. Flourishing Bioinspired Antifogging Materials with Superwettability: Progresses and Challenges. *Adv. Mater.* **2018**, 30, 1704652.
(4) Gam-Derouich, S.; Pinson, J.; Lamouri, A.; Decorse, P.; Bellynck, S.; Herbaut, R.; Royon, L.; Mangeney, C. Micro-Patterned Anti-Icing Coatings with Dual Hydrophobic/Hydrophilic Properties. *J. Mater. Chem. A* **2018**, 6, 19353−19357.
(5) Fan, P.; Bai, B.; Jin, G.; Zhang, H.; Zhong, M. Patternable Fabrication of Hyper-Hierarchical Metal Surface Structures for Ultrabroadband Antireflection and Self-Cleaning. *Appl. Surf. Sci.* **2018**, 457, 991−999.
(6) Walker, G. M.; Albadarin, A. B.; McGlue, A.; Brennan, S.; Bell, S. E. J. Analysis of Friction Factor Reduction in Turbulent Water Flow Using a Superhydrophobic Coating. *Prog. Org. Coat.* **2016**, 90, 472−476.
(7) Lee, J.; Heo, K.; Schulz-Schonhagen, K.; Lee, J. H.; Desai, M. S.; Jin, H.; Lee, S. Diphenylalanine Peptide Nanotube Energy Harvesters. *ACS Nano* **2018**, 12, 8138−8144.
(8) Almohammed, S.; Oladapo, S. O.; Ryan, K.; Kholkin, A. L.; Rice, J. H.; Rodriguez, B. J. Wettability Gradient-Induced Alignment of Peptide Nanotubes as Templates for Biosensing Applications. *RSC Adv.* **2016**, 6, 41809−41815.
(9) Hensel, R.; Neinhuis, C.; Werner, C. The Springtail Cuticle as a Blueprint for Omniphobic Surfaces. *Chem. Soc. Rev.* **2016**, 45, 323−341.
(10) Zhan, W.; Yu, S.; Gao, L.; Wang, F.; Fu, X.; Sui, G.; Yang, X. Bioinspired Assembly of Carbon Nanotube into Graphene Aerogel with "Cabbagelike" Hierarchical Porous Structure for Highly Efficient Organic Pollutants Cleanup. *ACS Appl. Mater. Inter.* **2018**, 10, 1093−1103.
(11) Gao, X.; Jiang, L. Water-Repellent Legs of Water Striders. *Nature* **2004**, 432, 36.
(12) David, R.; Neumann, A. W. Computation of the Wetting Properties of Randomly Structured Superhydrophobic Surfaces. *J. Phys. Chem. C* **2012**, 116, 16601−16608.
(13) Yong, J.; Yang, Q.; Chen, F.; Zhang, D.; Farooq, U.; Du, G.; Hou, X. A Simple Way to Achieve Superhydrophobicity, Controllable Water Adhesion, Anisotropic Sliding, and Anisotropic Wetting Based on Femtosecond-Laser-Induced Line-Patterned Surfaces. *J. Mater. Chem. A* **2014**, 2, 5499−5507.
(14) Tricinci, O.; Terencio, T.; Mazzolai, B.; Pugno, N. M.; Greco, F.; Mattoli, V. 3D Micropatterned Surface Inspired by Salvinia Molesta via Direct Laser Lithography. *ACS Appl. Mater. Inter.* **2015**, 7, 25560−25567.
(15) Yang, Y.; Li, X.; Zheng, X.; Chen, Z.; Zhou, Q.; Chen, Y. 3D-Printed Biomimetic Super-

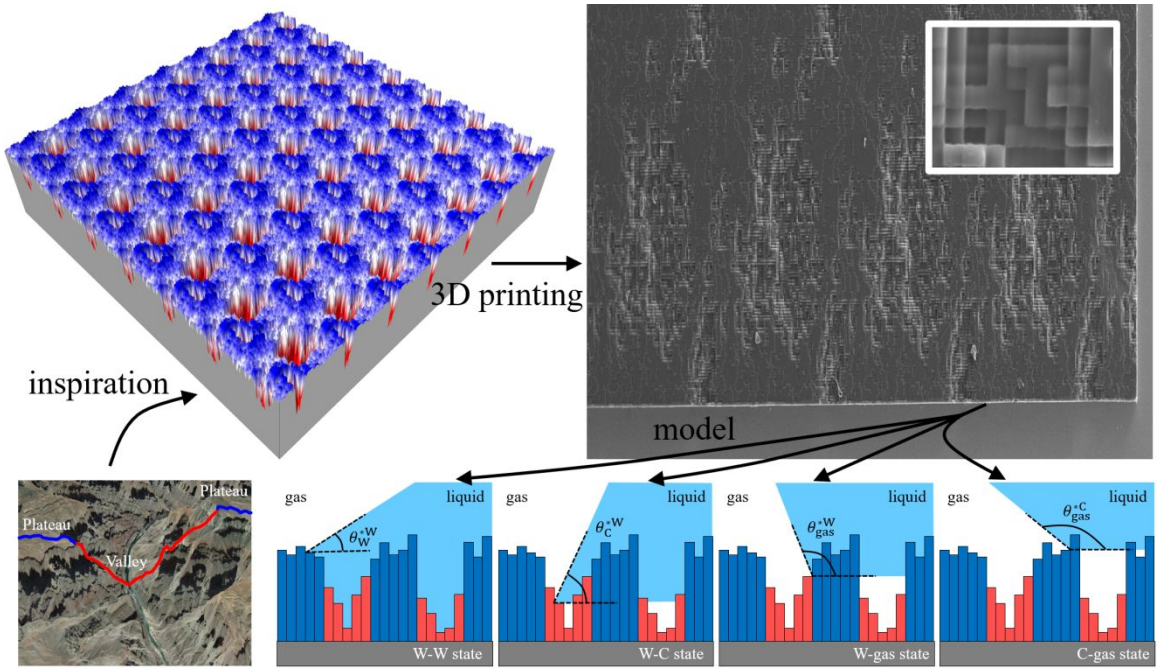
Hydrophobic Structure for Microdroplet Manipulation and Oil/Water Separation. *Adv. Mater.* **2018**, 30, 1704912.
(16) Liu, T.; Kim, C. Turning a Surface Superrepellent Even to Completely Wetting Liquids. *Science*, **2014**, 346, 1096−1100.
(17) Liu, X; Gu, H.; Wang, M.; Du, X.; Gao, B.; Elbaz, A.; Sun, L.; Liao, J.; Xiao, P.; Gu, Z. 3D Printing of Bioinspired Liquid Superrepellent Structures. *Adv. Mater.* **2018**, 30, 1800103.
(18) Mandlebrot, B. B. The Fractal Geometry of Nature, W. H. Freeman and Company: New York**,** 1982.
(19) Corral, I. B.; Calvet, J. V.; Salcedo, M. C. Use of Roughness Probability Parameters to Quantify the Material Removed in Plateau-Honing. *Int. J. Mach. Tools Manufact.* **2010**, 50, 621−629.
(20) Hu, S.; Brunetiere, N.; Huang, W.; Liu, X.; Wang, Y. The Bi-Gaussian Theory to Understand Sliding Wear and Friction. *Tribol. Int.* **2017**, 114, 186−191.
(21) Hu, S.; Reddyhoff, T.; Puhan, D.; Vladescu, S; Huang, W; Shi, X; Dini, D; Peng Z. Bi-Gaussian Stratified Wetting Model on Rough Surfaces. *Langmuir* **2019**, 35, 5967−5974.
(22) Vilaro, I.; Yague, J. L.; Borros, S. Superhydrophobic Copper Surfaces with Anticorrosion Properties Fabricated by Solventless CVD Methods. *ACS Appl. Mater. Inter.* **2017**, 9, 1057−1065.
(23) Jedlicka, S. S.; McKenzie, J. L.; Leavesley, S. L.; Little, K.M.; Webster, T. J.; Robinson, J. P.; Nivens, D. E.; Rickus, J. L. Sol-Gel Derived Materials as Substrates for Neuronal Differentiation: Effects of Surface Features and Protein Conformation. *J. Mater. Chem.* **2006**, 16, 3221−3230.
(24) Rahmawan, Y.; Xu, L.; Yang, S. Self-Assembly of Nanostructures Towards Transparent, Superhydrophobic Surfaces. *J. Mater. Chem. A* **2013**, 1, 2955−2969.
(25) Frenzel, T.; Kadic, M.; Wegener, M. Three-Dimensional Mechanical Metamaterials with A Twist. *Science* **2017**, 358, 1072−1074.
(26) Xiao, T. P.; Cifci, O. S.; Bhargava, S.; Chen, H.; Gissibl, T.; Zhou, W.; Giessen, H.; Toussaint, K. C.; Yablonovitch, E.; Braun, P. V. Diffractive Spectral-Splitting Optical Element Designed by Adjoint-Based Electromagnetic Optimization and Fabricated by Femtosecond 3D Direct Laser Writing. *ACS Photonics* **2016**, 3, 886−894.
(27) Sakellari, I.; Yin, X.; Nesterov, M. L.; Terzaki, K.; Xomalis, A.; Farsari, M. 3D Chiral Plasmonic Metamaterials Fabricated by Direct Laser Writing: The Twisted Omega Particle. *Adv. Opt. Mater.* **2017**, 5, 1700200.
(28) Hengsbach, S.; Lantada, A. D. Direct Laser Writing of Fractal Surfaces: Strategy to Design and Manufacture Textured Materials. *Adv. Eng. Mater.* **2015**, 17, 172−180.
(29) Davis, E.; Liu, Y.; Jiang, L.; Lu, Y.; Ndal, S. Wetting Characteristics of 3-Dimensional Nanostructured Fractal Surfaces. *Appl. Surf. Sci.* **2017**, 392, 929−935.
(30) Lantada, A. D.; Hengsbach, S.; Bade, K. Lotus-On-Chip: Computer-Aided Design and 3D Direct Laser Writing of Bioinspired Surfaces for Controlling the Wettability of Materials and Devices. *Bioinspir. Biomim.* **2017**, 12, 066004.
(31) Quere, D. Fakir droplets. *Nat. Mater.* **2002**, 1, 14−15.
(32) Hensel, R.; Neinhuis, C.; Werner, C. The Springtail Cuticle as a Blueprint for Omniphobic

Surfaces. Chem. Soc. Rev. **2016**, 45, 323−341.

(33) Hensel, R.; Helbig, R.; Aland, S.; Voigt, A.; Neinhuis, C.; Werner, C. Tunable Nano-Replication to Explore the Omniphobic Characteristics of Springtail Skin. *NPG Asia Mater.* **2013**, 5, e37.

(34) Geng, H.; Zhou, K.; Zhou, J.; Ma, H.; Lv, C.; Li, C.; Xu, Z.; Qu, L. Sunlight-Driven Water Transport via a Reconfigurable Pump. *Angew. Chem. Int. Edit.* **2018**, 130, 15661−15666.

TOC


3D printing
inspiration
model
Plateau
Plateau
Valley
gas
liquid
W-W state
W-C state
W-gas state
C-gas state

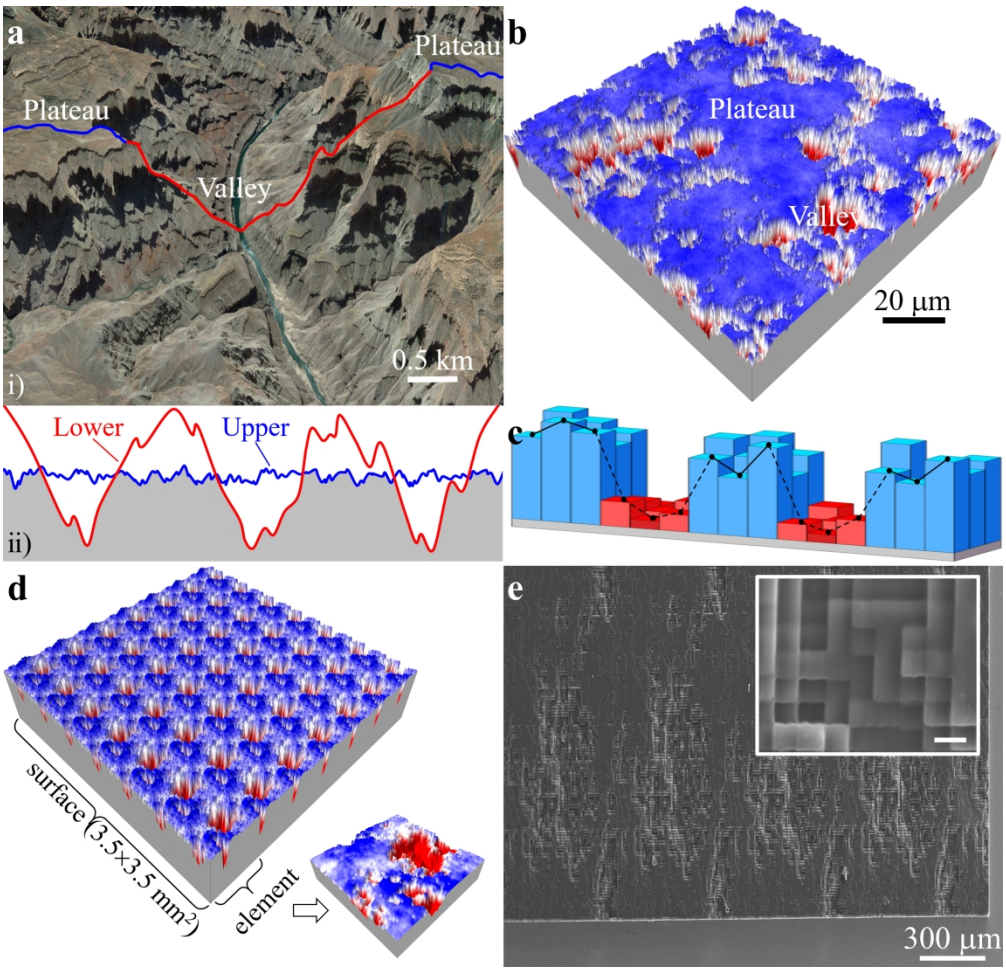


Figure 1

638x612mm (144 x 144 DPI)

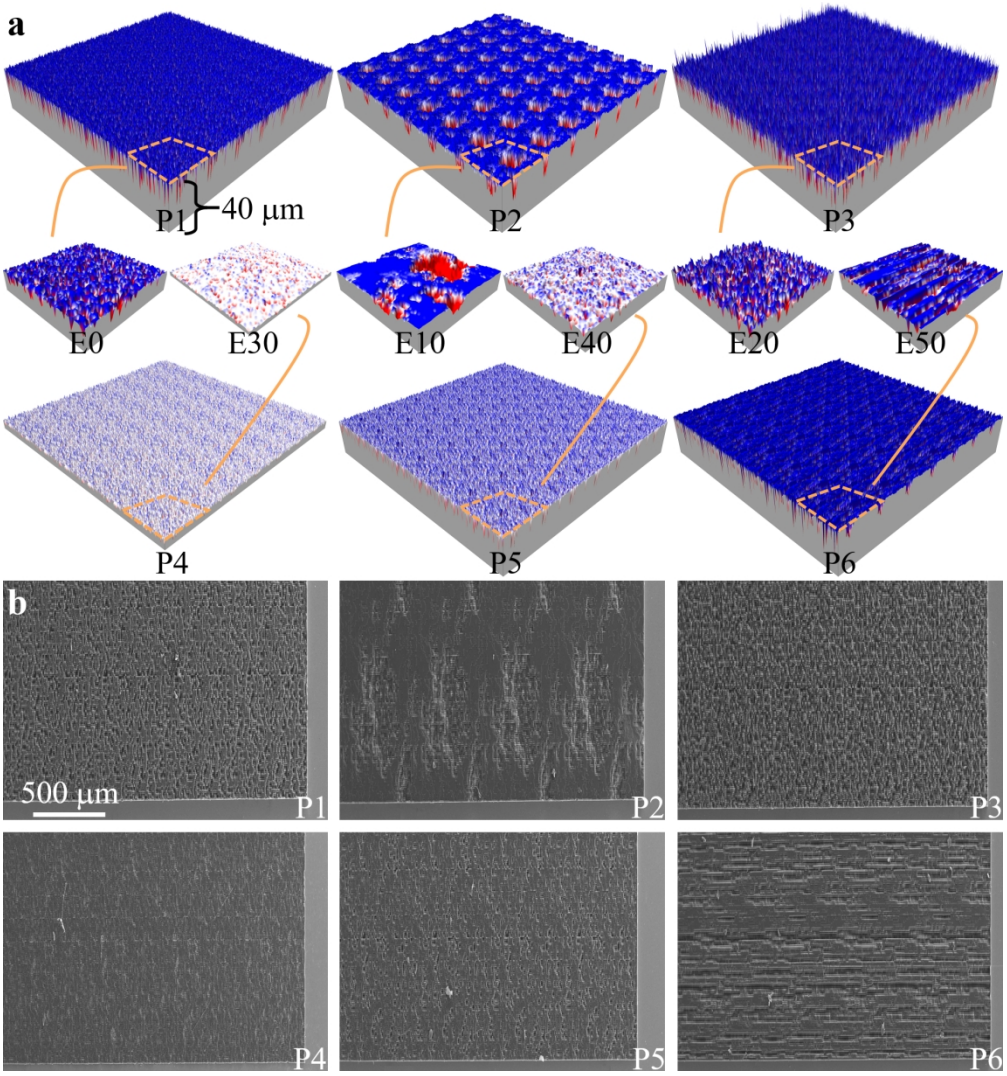


Figure 2

348x371mm (144 x 144 DPI)

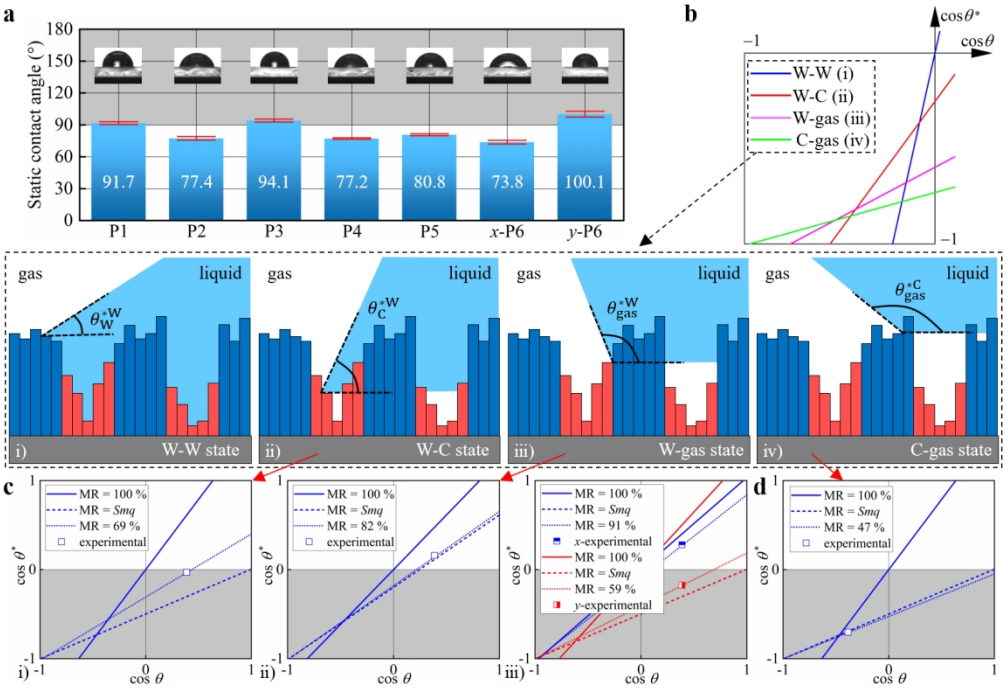


Figure 3

298x203mm (144 x 144 DPI)

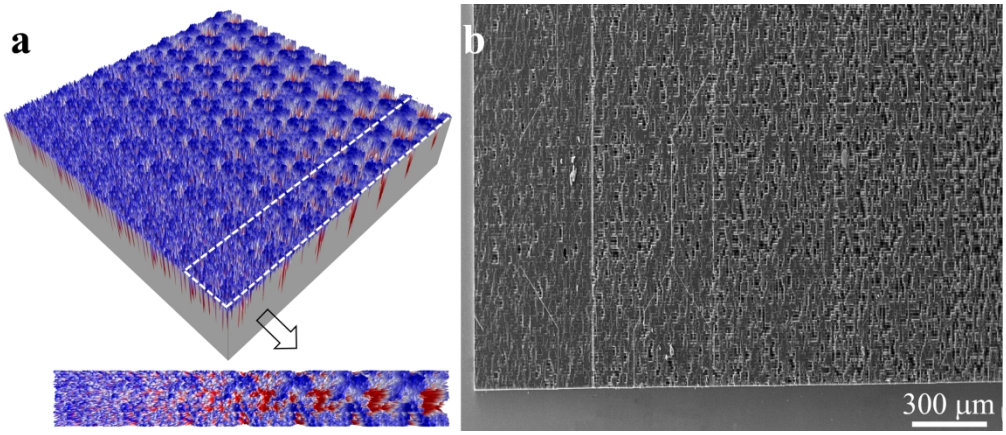


Figure 4

431x183mm (144 x 144 DPI)

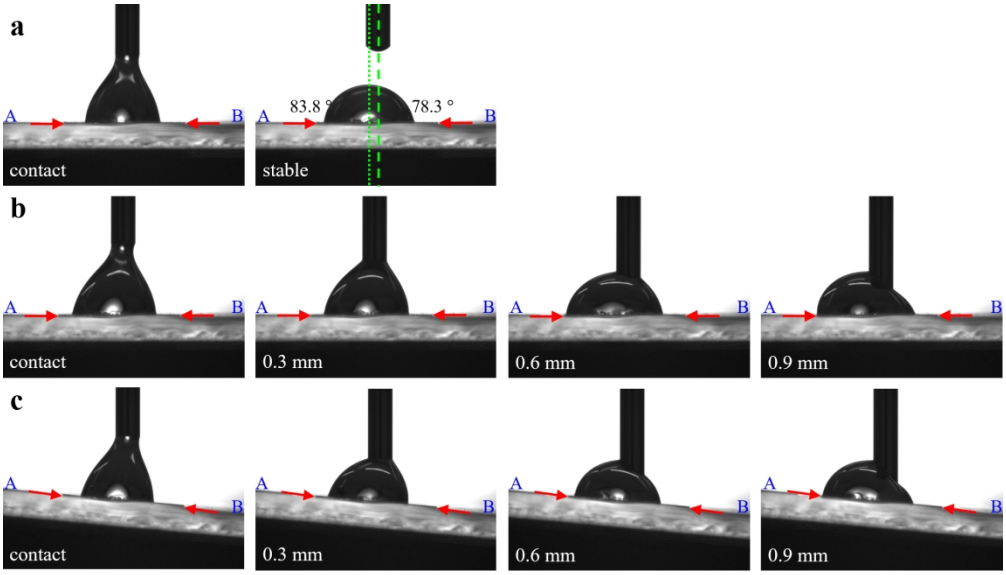


Figure 5

374x212mm (144 x 144 DPI)

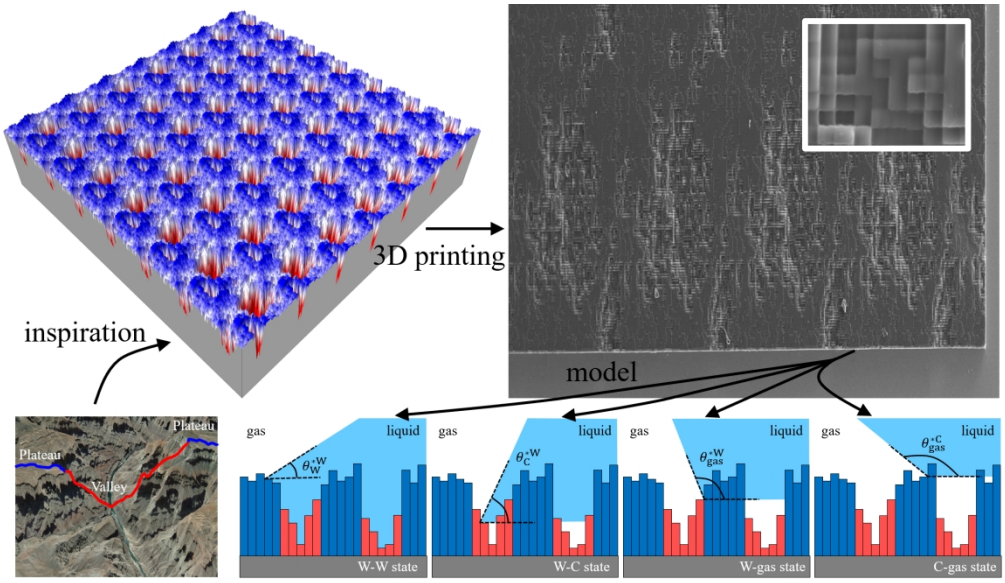


Figure TOC

386x222mm (144 x 144 DPI)